scientific reports

Check for updates

OPEN

Skyrmion-mediated nonvolatile ternary memory

Md Mahadi Rajib[1], Namita Bindal[2,3], Ravish Kumar Raj[2], Brajesh Kumar Kaushik[2] & Jayasimha Atulasimha[1,4]✉

Multistate memory systems have the ability to store and process more data in the same physical space as binary memory systems, making them a potential alternative to existing binary memory systems. In the past, it has been demonstrated that voltage-controlled magnetic anisotropy (VCMA) based writing is highly energy-efficient compared to other writing methods used in non-volatile nanomagnetic binary memory systems. In this study, we introduce a new, VCMA-based and skyrmion-mediated non-volatile ternary memory system using a perpendicular magnetic tunnel junction (p-MTJ) in the presence of room temperature thermal perturbation. We have also shown that ternary states {− 1, 0, + 1} can be implemented with three magnetoresistance values obtained from a p-MTJ corresponding to ferromagnetic up, down, and skyrmion state, with 99% switching probability in the presence of room temperature thermal noise in an energy-efficient way, requiring ~ 2 fJ energy on an average for each switching operation. Additionally, we show that our proposed ternary memory demonstrates an improvement in area and energy by at least 2X and ~ 10^4X respectively, compared to state-of-the-art spin-transfer torque (STT)-based non-volatile magnetic multistate memories. Furthermore, these three states can be potentially utilized for energy-efficient, high-density in-memory quantized deep neural network implementation.

In the field of computer technology, CMOS-based two-state memory is widely used. When evaluating memory systems, key considerations include writing and reading speed, reliability, endurance, non-volatility, high density, and energy-efficiency[1]. As CMOS-based two-state memory systems are volatile and are reaching their limits for high-density implementation, researchers are searching for alternatives. Currently, flash memory is the most advanced non-volatile option available, however, it has an endurance problem[1–3]. Other potential options that are still being researched include resistive random-access-memory (RRAM)[4], phase change memory (PCM)[5], magnetoresistive random-access memory (MRAM)[6,7] and ferroelectric random-access memory (FeRAM)[8,9] with MRAM being the most promising[1,10]. MRAM devices are made up of nanomagnets, where the "up" and "down" states typically represent the '0' and '1' bits in a p-MTJ as shown in Fig. 1a. There are two main methods to write these bits, a current-dependent method[11–14] and an electric field-dependent method[15–19]. The current-dependent approach typically results in high energy dissipation when switched with STT[11,12,20]. The use of spin–orbit torque (SOT) could potentially improve energy-efficiency; however, it requires a three terminal device geometry[13]. On the other hand, electric field-based write approach can be more energy-efficient whether mediated through strain[21–27] or voltage control of magnetic anisotropy[17,28,29] or other methods such as electrical switching of polarization coupled to antiferromagnetic state[30]. In particular, MTJs switched with strain can potentially be scaled to switch at < 1 fJ/bit[31] while voltage-controlled magnetic anisotropy-based switching, a type of electric field-dependent method, requires only a few fJ[32,33] of energy per switching operation compared to 100 fJ using STT switching (a current-dependent method)[34]. Along with energy-efficiency, high density of RAMs is also desirable, so a multi-state approach is more practical. In the past, multistate MRAM has been proposed using STT[35] and SOT[36], but these methods result in decreased density because they involve connecting MTJs in parallel or series. Three-terminal devices like SOT-MRAM require more space, and multibit STT-MRAM requires even more energy than its two-state counterpart. Therefore, there is a need to implement a multibit memory system in a single MTJ with two terminals in an energy-efficient way. Furthermore, ternary memory can be of utility for highly quantized deep neural networks (DNN).

In this study, a VCMA-based and skyrmion-mediated ternary memory system using a single MTJ with two terminals is presented. In addition to the standard "up" and "down" ferromagnetic states of the two-state MRAM

[1]Department of Mechanical and Nuclear Engineering, Virginia Commonwealth University, Richmond, VA 23284, USA. [2]Department of Electronics and Communication Engineering, Indian Institute of Technology Roorkee, Roorkee 247667, Uttarakhand, India. [3]Department of Electronics and Communication Engineering, MVJ College of Engineering, Bangalore 560067, India. [4]Department of Electrical and Computer Engineering, Virginia Commonwealth University, Richmond, VA 23284, USA. ✉email: jatulasimha@vcu.edu

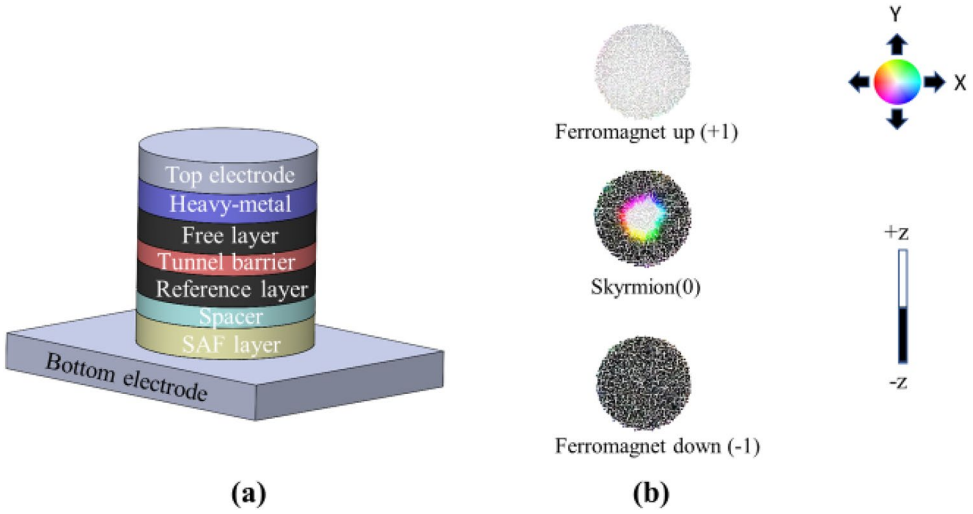

Figure 1. (**a**) Schematic of a magnetic tunnel junction with different constituent layers. The heavy-metal layer adjacent to the free layer creates Dzyaloshinskii-Moriya interaction (DMI) required for hosting skyrmions[60,61], and the synthetic antiferromagnetic (SAF) layer nullifies the effect of the reference layer on the free layer. (**b**) Ferromagnetic up, skyrmion and ferromagnetic down states represent + 1, ~ 0, − 1 states, respectively of the proposed ternary memory.

system, the third state in the proposed ternary memory system is a skyrmion state. In our system, the skyrmion state exhibits a conductance roughly equal to the average of the highest ("up" ferromagnetic state) and lowest ("down" ferromagnetic state) conductance values that is discussed in the "Results and discussions" section in detail. As a result, the skyrmion-mediated memory can be viewed as an almost balanced ternary memory, with resistance states of + 1 (ferromagnetic up), ~ 0 (skyrmion), and − 1 (ferromagnetic down). Here, we note that the magnetization of the reference layer is considered to be pinned in the upward direction.

Skyrmions are topologically protected states that offer nanoscale size, high velocity, and low depinning current density[37–39]. These spin textures are usually used in racetrack memory devices[38,40,41], but in this study, we propose the usage of a skyrmion in a confined structure like the MTJ. Our group has theoretically shown that switching between the ferromagnetic and skyrmion states in the MTJ's free layer can be done using VCMA at 0 K[42], and also experimentally shown that skyrmions can be created and annihilated in a thin film using VCMA[43]. However, the creation and annihilation of skyrmions at room temperature in a confined structure with VCMA has not been reported yet. This study theoretically demonstrates that a dense and energy-efficient ternary memory can be implemented by alternating between the three states (ferromagnetic up, ferromagnetic down, and skyrmion as shown in Fig. 1b) using VCMA in a patterned 100 nm nanodot in the presence of thermal noise at room temperature. We have shown in other work that such skyrmion-mediated VCMA-based two-state memory can be scaled to < 50 nm[44,45] which suggests that this approach also has the potential for scalable ternary memory.

The proposed three state memory system can also be used for implementing neuromorphic computing devices, particularly as quantized synaptic weights for DNN. The demand for neuromorphic computing is growing rapidly due to its ability to handle training and inference tasks in energy-limited environments like edge devices[46–48]. In DNN, the aspect that requires the most time and energy is the vector–matrix multiplication operation[49]. In-memory computing offers a more efficient and low-energy solution to this challenge[48]. The previously mentioned non-volatile memory types, such as MRAM[50–52], flash memory[53], RRAM[54,55], and PCM[56,57], have been also shown to be useful in performing multiply-accumulate operations commonly found in artificial neural networks[58]. Of these, MRAM has been extensively researched for its high endurance, low energy requirements for reading and writing, non-volatility, and compatibility with CMOS technology[51,59]. Recently, it has been demonstrated that use of three or five-state domain wall based quantized synaptic weights in DNN can perform recognition tasks with an accuracy comparable to that of floating-point precision synaptic weight based DNNs with low energy consumption[51]. However, writing multiple states in domain wall-based racetrack devices requires a lot of space. In this study, we also discuss that our proposed three-state memory system, implemented in a two-terminal MTJ, allows for the potential implementation of quantized synaptic weights with a comparable energy consumption to domain wall-based DNNs, but with significantly less space requirements.

Results and discussion

There are three different switching operations that are primarily carried out: switching from a ferromagnet (+ 1/− 1) to a skyrmion state (0), switching from a skyrmion (0) to a ferromagnet state (+ 1/− 1), and switching from one ferromagnet (+ 1/− 1) to another (− 1/ + 1). Here, we note that the reference layer is magnetized in the upward direction in the p-MTJ. Therefore, the ferromagnetic up and down state has the highest and lowest conductance, respectively, while the skyrmion state has an intermediate conductance between the highest and lowest[62], which is nearly half of the combined conductance in the case of skyrmions with equal number of up

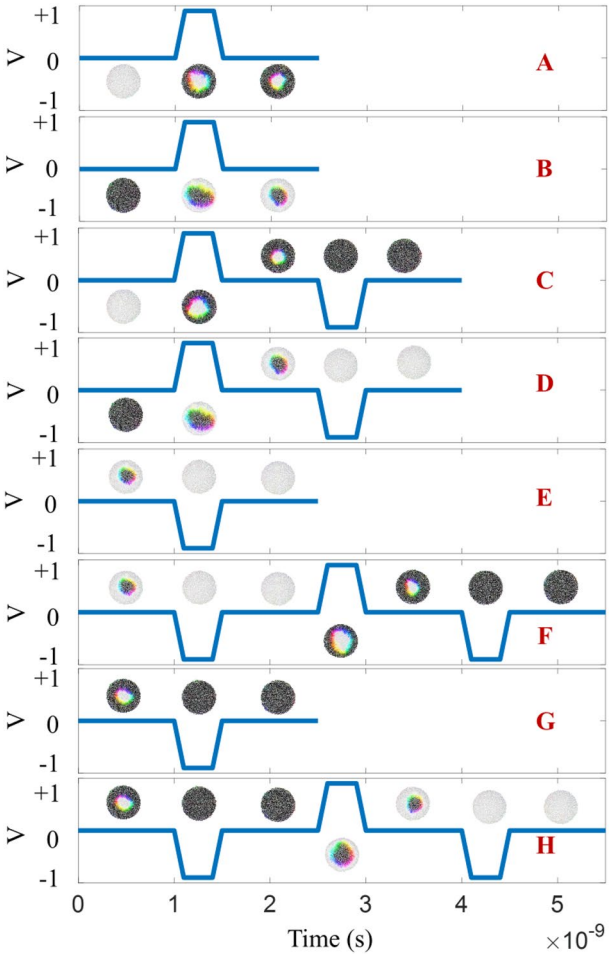

Figure 2. Applied voltage vs time for different switching cases (the magnetization states for different voltage pulses are shown correspondingly).

and down spins. This allows the execution of all six interconversions needed to implement a three-state memory. However, as shown in Fig. 2, eight situations occur while performing switching operations.

In case A, switching from ferromagnetic up (+1) to skyrmion state (0) is performed. For performing this switching operation, the ferromagnetic up state is relaxed for 1 ns and perpendicular magnetic anisotropy (PMA) energy is reduced from 1.5 to 1.05 MJ/m^3 in 0.1 ns by applying a + 1 V pulse. Here, we note that it has been previously experimentally observed that positive voltage pulse reduces PMA while negative voltage pulse increases PMA[43,63]. When the PMA is reduced, the presence of DMI field in the ferromagnetic free layer creates a skyrmion state of polarity − 1. Here, we note that the skyrmion polarity can be defined as $p = [m_z (r = \infty) - m_z (r = 0)]/2$[64]. Therefore, skyrmion with boundary (core) pointing down (up) and core (boundary) pointing up(down) has polarity − 1 (+1). We observe that when the PMA is reduced from the ferromagnetic up state, a skyrmion of polarity − 1 is created because the boundary spins tilt in the opposite direction from the core spins and the core spins are in their starting spin orientation. The voltage pulse is applied for 0.3 ns and subsequently withdrawn in 0.1 ns to restore the initial PMA of 1.5 MJ/m^3. We observe that the skyrmion state is stabilized after the withdrawal of the voltage pulse. Thus, by applying and subsequently withdrawing a + 1 V pulse, a skyrmion state (0) can be created and stabilized starting from a ferromagnetic up state (+1).

In case B, we start from a ferromagnetic down state (− 1) and when PMA is reduced in 0.1 ns by applying a + 1 V pulse, a skyrmion of polarity + 1 is created. The skyrmion created in this instance has the opposite polarity of the one created in case A because we start from the opposite ferromagnetic state i.e. the ferromagnetic down state. Thus, switching from ferromagnetic down to skyrmion state can be accomplished in a single step similar to case A.

In case C, ferromagnetic up state is switched to ferromagnetic down state. This is a two-step operation. First, a + 1 V pulse is applied to reduce the PMA and create a skyrmion state. The created skyrmion has core oriented in the upward direction and boundary in the downward direction. When a − 1 V pulse is applied to increase the PMA from 1.5 to 1.95 MJ/m^3 in 0.1 ns, the skyrmion annihilates to the ferromagnetic down state following the skyrmion's downward oriented boundary spins. This switching is deterministic since ferromagnetic up state is switched to ferromagnetic down state through an intermediate skyrmion state which has downward oriented boundary spin and the skyrmion annihilates to ferromagnetic down state following the boundary

spins' orientation. We can see from Fig. 2 that the ferromagnetic down state is stable after the PMA is restored by withdrawing the + 1 V pulse.

Similarly, in case D, ferromagnetic down state is switched to ferromagnetic up state through an intermediate skyrmion state. In this case, starting from a ferromagnetic down state, an intermediate skyrmion with boundary spin in the upward direction and core in the downward direction is created by applying + 1 V pulse and subsequently the skyrmion is annihilated to ferromagnetic up state by applying − 1 V pulse. Therefore, writing − 1/ + 1 to + 1/− 1 is a two-step operation where a positive and a negative voltage pulse is applied sequentially.

Writing from skyrmion to ferromagnet can be one step/three step operation. We have seen in case C and case D that while switching from one ferromagnetic to other ferromagnetic state through an intermediate skyrmion state, the skyrmion state annihilates to ferromagnetic state following the skyrmion state's boundary spin orientation. Writing a desired ferromagnetic state from a skyrmion state can be a one-step or three-step operation depending on the skyrmion polarity because we can't tell the skyrmion's polarity from its magnetoresistance value. For example, if the skyrmion has upward oriented boundary spin then it will annihilate to a ferromagnetic up state (case E). But, if the desired state is the downward ferromagnetic state then the ferromagnetic up state is required to be switched by following the similar operations performed in case C and case D.

In case E, we can see that skyrmion with boundary spin in the upward direction can be switched to a ferromagnetic up state by applying a − 1 V pulse. If the desired state is ferromagnetic down state then a sequential application of + 1 V and − 1 V pulse will switch the ferromagnetic up state to ferromagnetic down state requiring a three- step operation overall which is shown in case F. If the initial state is a skyrmion state with downward boundary spin and a ferromagnetic down state needs to be written, then the application of a + 1 V pulse completes the switching as shown in case G. If the desired state is ferromagnetic up state then a sequential application of + 1 V and − 1 V pulse will be required to switch the ferromagnetic down state to ferromagnetic up state as shown in case H.

We note that for implementing the switching operations, one of the key steps is the creation of a skyrmion, whether it involves transitioning from a ferromagnetic state to a skyrmion state or switching between two different ferromagnetic states. The skyrmion is created following the method in ref[65]. In this process, when a voltage pulse is applied, the perpendicular magnetic anisotropy (PMA) is reduced, leading to the creation of a dynamic skyrmion. This dynamic skyrmion subsequently annihilates, transitioning to the opposite ferromagnetic state when the pulse is withdrawn. However, in our approach, since skyrmion stabilization is necessary, we choose such an initial PMA value that when it is reduced, a dynamic skyrmion is created but it remains in that skyrmion state when the PMA is restored rather than being annihilated as illustrated in ref[65]. For demonstrating the skyrmion creation method, we started from a ferromagnetic up state for various initial PMA which are stabilized for 1 ns. Then, a positive voltage pulse is applied which reduces the PMA and creates a dynamic skyrmion state. We note that the skyrmion state can be realized from topological charge/winding number which is defined as $N=\frac{1}{4\pi}\int(\frac{\partial\vec{m}}{\partial x}\times\frac{\partial\vec{m}}{\partial y}).\vec{m}\,dxdy$[66]. We also note that ferromagnetic and skyrmion states are represented by a topological charge 0 and ~ 1, respectively. In Fig. 3, we can observe that when the initial PMA is > 1.6 MJ/m^3, the skyrmion annihilates upon the withdrawal of the voltage pulse, transitioning to the opposite ferromagnetic state. However, when the initial PMA is below that value, the skyrmion is stabilized after the voltage pulse is withdrawn. Therefore, the created dynamic skyrmion can be trapped in a stable state when the initial PMA is chosen to be less than a threshold PMA (see Supplementary Information section S1 for the stability of the skyrmion state). We note that for implementing skyrmion-mediated non-volatile ternary memory, we considered 1.5 MJ/m^3 as the initial PMA value.

We ran simulations for 1000 times to study the switching percentage in each of the eight cases in the presence of room temperature thermal perturbation, and the results are shown in Table 1. On average, switching

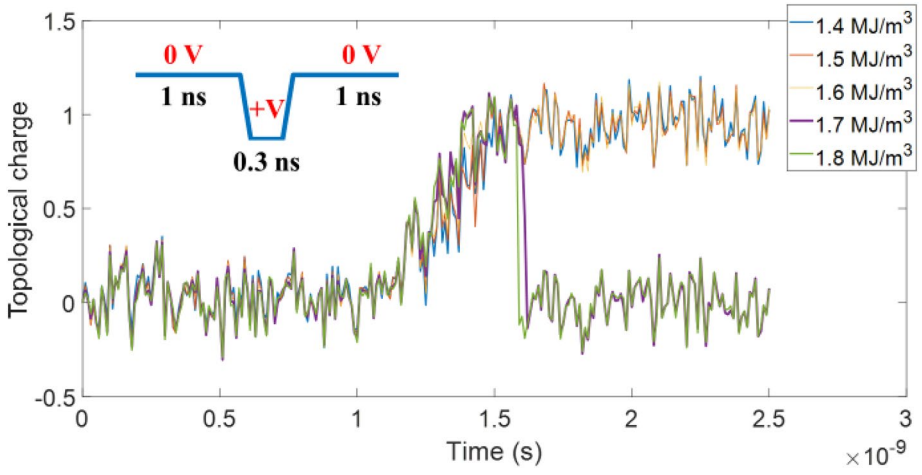

Figure 3. The ferromagnetic up state is stabilized for 1 ns and the initial PMA is reduced in 0.1 ns by applying positive voltage which is restored after 0.3 ns by withdrawing the voltage pulse (The pulse is shown inset). Different colors represent the change in topological charge during the application of voltage pulse for various initial PMA values.

Case	Switching percentage	Write energy (fJ)	Read energy (fJ)	Total energy (fJ)
Case A	98.70	0.337	1.595	1.932
Case B	98.70	0.337	1.192	1.529
Case C	98.80	1.011	1.569	2.58
Case D	99.00	1.011	1.569	2.58
Case E	100	0.337	1.595	1.932
Case F	99.10	1.685	1.192	2.877
Case G	100	0.337	1.192	1.529
Case H	98.9	1.685	1.192	2.877

Table 1. Switching percentage and energy dissipation for performing different switching operations.

occurred in ~ 99% of the cases (see Supplementary Information section S2 for the effect of process variation on switching percentage).

Energy dissipation

We calculated the energy required for each switching operation considering all of the reading and writing operations involved. For calculating the energy dissipation, the conductance of the device is obtained by calculating the conductance of the MTJ-like structure using[67,68]:

$$G_{device} = G_0 \sum_i \frac{1 + P^2 cos\theta_i}{1 + P^2} \tag{1}$$

where P is the spin polarization, and $G_0 = 1.1219$ mS denotes the conductance when all the spins of the free layer (FL) and reference layer (RL) of the MTJ are perfectly parallel to each other. We determine G_0 by considering the resistance area product of the p-MTJ, RA = 7 Ωμm[269], and the resistance for the parallel orientation of the free and fixed layer, $R_p = 891.27$ Ω. In Eq. (1), θ_i denotes the angle between the magnetization of the ith cell of the FL and the corresponding cell at the RL. From Eq. (1), we obtain effective resistance (numerical calculations using the .ovf files from the simulations) of the ferromagnetic up and ferromagnetic down states as 901.765 Ω and 2127 Ω, respectively, and the average resistance of the skyrmion state as 1376 Ω.

While implementing skyrmion-mediated ternary memory, energy is dissipated during both the reading and writing processes that involves $I_{read}{}^2 R_{MTJ} t_{read}$ and $\frac{1}{2} C V_{write}^2$ loss, respectively. To read the states, a 600 mV pulse is applied for 1 ns, while different combinations of read and write pulses are applied to write different states. For example, in case A, the initial and final states are read as ferromagnetic up state, and the skyrmion state, respectively and the energy dissipated for reading is 0.986 fJ and 0.609 fJ, respectively, thus the total energy dissipated for reading is 1.595 fJ. To write the skyrmion state, a + 1 V is applied for 0.5 ns, resulting in 0.337fJ of switching energy. Therefore, operating case A requires a total of 1.932 fJ of energy. Table 1 shows the energy required for switching from one state to another for all eight cases. On average, the energy dissipated in writing the three states is 2.20 fJ. Here, we note that considering the reference layer's magnetization pinned in the upward direction, the energy dissipated in reading the individual ferromagnetic up, ferromagnetic down, and skyrmion states are 0.986 fJ, 0.583 fJ, and 0.609 fJ, respectively. The read circuit used for calculating the energy dissipated while reading those states, created following the method illustrated in reference[70], is shown in Fig. 4.

As shown in Fig. 4, the Pre-Charge Sense Amplifier (PCSA) is used to read the values stored in MTJ -based ternary devices[70–72]. This reading is based on the difference between the resistance of MTJ_{in} and R_{ref1}/R_{ref2}, which is determined by the magnetization orientation of the free-layer in comparison to that of fixed-layer. The three states of magnetization of MTJ_{in} i.e. parallel, antiparallel, and skyrmion states are read using two reference resistance i.e. R_{ref1} and R_{ref2} with values as 1.138 kΩ and 1.751 kΩ, respectively along with two PCSAs. When MTJ_{in} is in the parallel state, its resistance is 0.901 kΩ which is compared with R_{ref1} (1.138 kΩ). Thus, P2 turns to low and P1 to high, resulting in $OUT_1 = 1$ and EN = 0, thereby rendering the second PCSA inactive. When the MTJ_{in} is the skyrmion state, the resistance value is 1.376 kΩ and it is first compared with MTJ_{ref1} (1.138kΩ). Thus, P2 and P1 turns to high and low, respectively. This leads to $OUT_1 = 0$ and EN = 1 which activates the second PCSA. Now, the resistance value is compared with R_{ref2} (1.751 kΩ) that turns P3 to low and P4 to high that results in $OUT_2 = 1$. When MTJ_{in} is in antiparallel state having resistance value of 2.101 kΩ, compared with R_{ref1} and R_{ref2}, P2 turns to high and P1 to low. This results in $OUT_1 = 0$ and EN = 1, activating the second PCSA and that turns P3 and P4 to high and low, respectively. This further results in $OUT_2 = 0$ and $OUT_3 = 1$. In this way, the three states of the ternary memory can be read using two PCSAs with two reference resistances.

Previously, non-volatile multistate memories (3 or 4 states) were proposed using STT or SOT current, and these memories were created by arranging the MTJs in series or parallel configurations[35,36,73]. Therefore, implementing multistate memories with STT and SOT current requires at least twice the area of our proposed multistate memory, as shown in Table 2.

To estimate the current required for binary switching from the ferromagnetic upward to the ferromagnetic downward direction, akin to case C in our proposed ternary memory device, we consider a device structure similar to that of our proposed VCMA-based skyrmion-mediated ternary memory device. The STT current was determined using Slonczewski Λ parameter and Slonczewski secondary STT term ε' as 1 and 0, respectively[14]. By

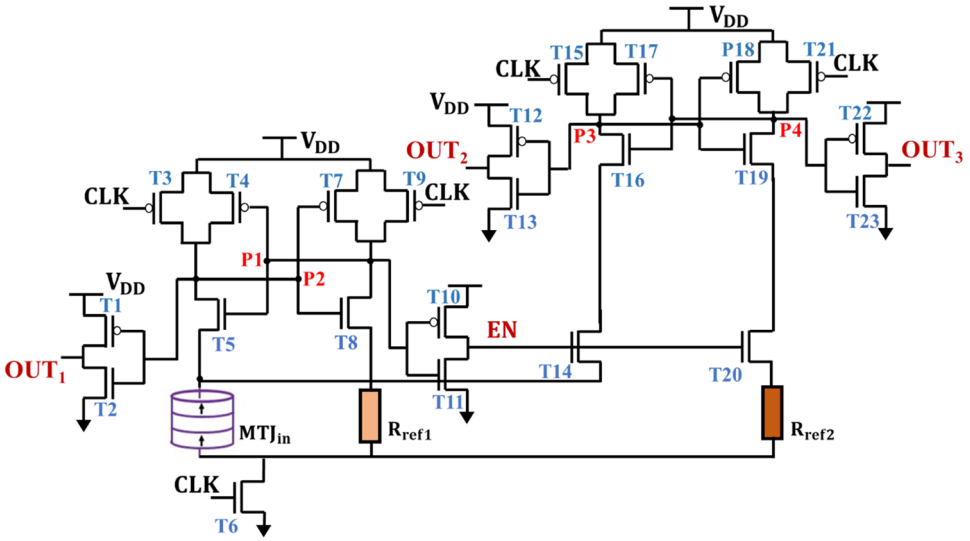

Figure 4. Schematic diagram of sense amplifier circuit used for reading p-MTJ states. Here, P and T represents terminals and transistors respectively.

	STT-based two state memory	STT-based multistate memory	DW-based stochastic multistate	Skyrmion-mediated ternary memory
Number of terminals	2	2	≥ 4[51,73]	2
Area	X	2X[73]	~ 4.5X[51]	X
Energy	~ 100 pJ	~ 200 pJ	~ 3 fJ[51]	~ 2 fJ

Table 2. Comparison of different multistate systems.

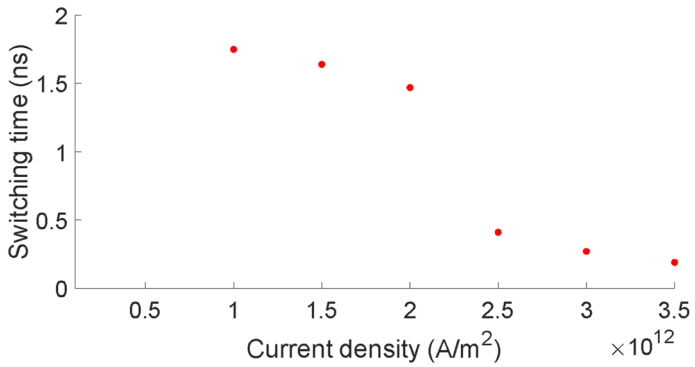

Figure 5. Switching time vs current density for ferromagnetic reversal with STT current.

applying STT current pulses of different densities for 5 ns, we observe that a minimum current density of 10^{12} A/m^2 is required for the ferromagnetic reversal, and the corresponding switching time is 1.75 ns, as shown in Fig. 5. We can also observe in Fig. 5 that with increasing current density, the switching time decreases. However, considering the minimum current required for implementing binary switching with STT current, the dissipated energy is 96.2 pJ, which is four orders of magnitude higher than the energy dissipated for implementing similar switching with VCMA. It is worth noting that in STT/SOT-based multistate memories, two consecutive switching operations are performed to write a single state, resulting in latency issues[73]. Therefore, considering the energy required for performing a switching operation with STT current in a single MTJ with a 100 nm diameter, which is same as the dimension of our proposed device, writing a state in a multistate STT-MRAM would require ~ 200 pJ of energy. On the other hand, although SOT memories require less energy than STT for an MTJ of similar diameter[74] for writing each bit, the requirement of three terminals reduces the density. Thus, our proposed

ternary memory achieves at least a 2X improvement in footprint and a four order of magnitude improvement in energy-efficiency compared to STT-based multistate memory.

We note that instead of adopting the two MTJs in series/parallel configuration, as shown in prior studies for the realization of ternary/multistate memories using STT current, an alternative approach involves the potential implementation of a skyrmion-mediated STT-current-based ternary memory. Though this alternative approach would potentially yield a similar device size to that of our proposed ternary memory, but it would require four orders of magnitude higher energy. Additionally, as the creation of a skyrmion forms a pivotal step in enabling skyrmion-mediated ternary memory, the process necessitates appropriate pulse shaping—an aspect that falls beyond the scope of our current study.

With an appropriate choice of material parameters, there is still the possibility of reducing the write error rate in the proposed ternary memory in the presence of room temperature thermal noise, as demonstrated in VCMA-based switching in ref[44,45]. However, the proposed three-state memory system, which achieves ~ 99% switching accuracy, has the potential to be utilized as quantized synaptic weights for DNNs. The previous idea to use three-state domain wall-based quantized synaptic weights achieved similar levels of accuracy during testing as floating-point precision synaptic weights[51]. However, the implementation of the three states requires a large racetrack (600 nm × 60 nm)[51], and the use of five terminals reduces the density significantly. Our proposed three-state memory system, which uses a single two-terminal MTJ, provides a way to implement quantized synaptic weights that consume similar amounts of energy as domain wall-based DNNs, but with significantly less space requirement (~ 4.5 times less space for the MTJ alone) as shown in Table 2.

In summary, we showed that a novel skyrmion-mediated ternary memory can be implemented in a p-MTJ in the presence of room temperature thermal noise. We also showed that our proposed ternary memory achieves at least a 2X improvement in footprint and a ~ 10^4 X improvement in energy-efficiency, respectively compared to STT-based multistate memory. By utilizing energy-efficient VCMA switching mechanism and employing a two-terminal MTJ device, our proposed memory design allows for the implementation of three distinct states within a single MTJ, thereby increasing both the cell density and the density of the peripheral circuit. Previously, it has also been theoretically shown that skyrmions can be scaled down to ~ 20 nm in a circular patterned nanodot[45], which could lead to even greater memory density in the future. Furthermore, three state synapses can be built with comparable energy costs and reduced space requirements (~ 4.5 times less area) compared to domain wall-based quantized DNNs.

For the experimental realization of voltage-controlled skyrmion-mediated ternary memory, one key step is the creation of a stable skyrmion and its annihilation with voltage in an MTJ. Recently, a couple of experimental works demonstrated the voltage-controlled creation of a skyrmion in an MTJ with CoFeB-based free and fixed layers and W/Pt-based heavy metal layers adjacent to the free layer, which creates DMI for hosting the skyrmion[60,61]. Apart from imaging skyrmions in an MTJ, it has been shown that skyrmions can be electrically read[60,61]. Building on these observations, the proposed skyrmion-mediated ternary memory can be experimentally realized.

Methods

We simulate the magnetization dynamics of the free layer of the circular shaped p-MTJs with a diameter of 100 nm which are discretized into 50 × 50 × 1 cells to observe the switching between three states and evaluate the switching probability of each switching case. The simulation uses the MuMAX3 program[75] to solve the magnetization dynamics based on Landau–Lifshitz–Gilbert–Slonczewski equation that is defined as follows:

$$\frac{\partial \vec{m}}{\partial t} = \left(\frac{-\gamma}{1+\alpha^2}\right)\left[\vec{m} \times \vec{B}_{eff} + \alpha\left\{\vec{m} \times \left(\vec{m} \times \vec{B}_{eff}\right)\right\}\right] + \beta\frac{\epsilon - \alpha\epsilon'}{1+\alpha^2}(\vec{m} \times (\vec{m_p} \times \vec{m})) - \beta\frac{\epsilon - \alpha\epsilon'}{1+\alpha^2}(\vec{m} \times \vec{m_p}) \tag{2}$$

$$\beta = \frac{j_z \hbar}{M_S e d} \tag{3}$$

$$\epsilon = \frac{P\Lambda^2}{(\Lambda^2+1) + (\Lambda^2-1)(\vec{m}.\vec{m_p})} \tag{4}$$

where α and γ denote the Gilbert damping coefficient and gyromagnetic ratio, respectively. $\vec{m}$ indicates the normalized magnetization vector with components m_x, m_y, and m_z along x, y, and z direction, respectively, which is obtained by normalizing the magnetization vector ($\vec{M}$) with respect to saturation magnetization (M_s). In Eqs. (2) and (3), j_z is the current density along the z axis, d is the thickness of the free layer, P is the spin polarization, $\vec{m_p}$ is the fixed-layer magnetization, the spacer layer is characterized by the Slonczewski Λ parameter and $\epsilon\prime$ is the secondary spin-torque parameter. The circular shaped free layers are divided into grids with dimensions of 2 nm × 2 nm × 1.5 nm, which are much smaller than the exchange length ($\sqrt{\frac{2A_{ex}}{\mu_0 M_S^2}}$). In Eq. (2), $\vec{B}_{eff}$ is the effective magnetic field having the following components:

$$\vec{B}_{eff} = \vec{B}_{demag} + \vec{B}_{exchange} + \vec{B}_{DM} + \vec{B}_{anis} + \vec{B}_{thermal} \tag{5}$$

In Eq. (5), $\vec{B}_{demag}$ represents the effective field due to demagnetization energy and $\vec{B}_{exchange}$ denotes the Heisenberg exchange interaction.

$\vec{B}_{DM}$ is the effective field due to DMI, which is expressed as follows:

Saturation magnetization (M_s)	1.3×10^{6} A/m[78]
Exchange stiffness (A_{ex})	20×10^{-12} J/m[79]
DMI	3.0×10^{-3} J/m^2[80]
Thickness (d)	1.5 nm
Damping coefficient	0.1[81]
Perpendicular magnetic anisotropy	1.5 MJ/m^3[60,82]
VCMA coefficient	675 fJ/Vm[82]
Spin polarization	0.65[83]
Oxide thickness	1 nm[84]

Table 3. Material properties.

$$\overrightarrow{B}_{DM} = \frac{2D}{M_s}\left(\frac{\partial m_z}{\partial x}, \frac{\partial m_z}{\partial y}, -\frac{\partial m_x}{\partial x} - \frac{\partial m_y}{\partial x}\right) \tag{6}$$

where D represents the DMI constant.

The perpendicular anisotropy ($\overrightarrow{B}_{anis}$) is expressed by the following equation:

$$\overrightarrow{B}_{anis} = \frac{2K_{u1}}{M_s}\left(\overrightarrow{u}.\overrightarrow{m}\right)\overrightarrow{u} \tag{7}$$

where K_{u1} and $\overrightarrow{u}$ represent the first order uniaxial anisotropy constant and unit vector in the anisotropy direction respectively.

The following equation is used to introduce the thermal field:

$$\overrightarrow{B}_{thermal} = \overrightarrow{\eta}\,(step)\sqrt{\frac{2\alpha k_B T}{M_s \gamma \Delta V \Delta t}} \tag{8}$$

where T is the temperature (K), ΔV is the cell volume, k_B is the Boltzmann constant, Δt is time step and $\overrightarrow{\eta}$ (step) is a random vector from a standard normal distribution. Here, we note that the random vector $\overrightarrow{\eta}$ is independent (uncorrelated) for each of the three Cartesian coordinates and is generated at every time step.

VCMA coefficient is calculated using the following equation[65,76,77]:

$$\zeta = \frac{\Delta PMA \times d}{(V/t_{MgO})} \tag{9}$$

where ΔPMA is the required modulation of PMA, d is the free layer thickness, V is the applied voltage pulse and t_{MgO} is the thickness of the oxide layer.

The parameters for Co based magnetic materials are used for the simulation of magnetization dynamics of the skyrmions that are given in Table 3 (Supplementary Information S1).

Data availability

The datasets used and/or analysed during the current study available from the corresponding author on reasonable request.

Received: 17 November 2023; Accepted: 4 July 2024
Published online: 26 July 2024

References

1. Chen, A. A review of emerging non-volatile memory (NVM) technologies and applications. *Solid-State Electron.* **125**, 25–38 (2016).
2. Banerjee, W. Challenges and applications of emerging nonvolatile memory devices. *Electronics.* **9**, 1029 (2020).
3. Wang, K. L., Alzate, J. G. & Amiri, P. K. Low-power non-volatile spintronic memory: STT-RAM and beyond. *J. Phys. D Appl. Phys.* **46**, 074003 (2013).
4. Lee, H. Y. *et al.* Low power and high speed bipolar switching with a thin reactive Ti buffer layer in robust HfO2 based RRAM. In *IEEE International Electron Devices Meeting*, 1–4. https://doi.org/10.1109/IEDM.2008.4796677 (2008)
5. Burr, G. W. *et al.* Phase change memory technology. *J. Vacuum Sci. Technol. B Nanotechnol. Microelectron. Mater. Process. Meas. Phenomena* **28**, 223–262 (2010).
6. Valet, T. & Fert, A. Theory of the perpendicular magnetoresistance in magnetic multilayers. *Phys. Rev. B.* **48**, 7099 (1993).
7. Moodera, J. S., Kinder, L. R., Wong, T. M. & Meservey, R. Large magnetoresistance at room temperature in ferromagnetic thin film tunnel junctions. *Phys. Rev. Lett.* **74**, 3273 (1995).
8. Amanuma, K *et al.* Capacitor-on-metal/via-stacked-plug (CMVP) memory cell for 0.25/spl mu/m CMOS embedded FeRAM. In *International Electron Devices Meeting, Technical Digest (Cat. No. 98CH36217)*, 363–366; https://doi.org/10.1109/IEDM.1998.746375 (1998).
9. Jones, R. E. Ferroelectric nonvolatile memories for embedded applications. In *Proceedings of the IEEE 1998 Custom Integrated Circuits Conference (Cat. No. 98CH36143)*, 431–438; https://doi.org/10.1109/CICC.1998.695013 (1998).
10. Avalanche technology. https://www.avalanche-technology.com/technology/mram-technology/.
11. Slonczewski, J. C. Current-driven excitation of magnetic multilayers. *J. Magn. Magn. Mater.* **159**, L1–L7 (1996).
12. Berger, L. Emission of spin waves by a magnetic multilayer traversed by a current. *Phys. Rev. B.* **54**, 9353 (1996).
13. Liu, L. *et al.* Spin-torque switching with the giant spin Hall effect of tantalum. *Science.* **336**, 555–558 (2012).

14. Misba, W. A., Rajib, M. M., Bhattacharya, D. & Atulasimha, J. Acoustic-wave-induced ferromagnetic-resonance-assisted spin-torque switching of perpendicular magnetic tunnel junctions with anisotropy variation. *Phys. Rev. Appl.* **14**, 014088 (2020).
15. Shiota, Y. *et al.* Induction of coherent magnetization switching in a few atomic layers of FeCo using voltage pulses. *Nat. Mater.* **11**, 39–43 (2012).
16. Amiri, P. K., & Wang, K. L. Voltage-controlled magnetic anisotropy in spintronic devices. *Spin*. **2**, 03, 1240002 (2012).
17. Wang, W. G., Li, M., Hageman, S. & Chien, C. L. Electric-field-assisted switching in magnetic tunnel junctions. *Nat. Mater.* **11**, 64–68 (2012).
18. Maruyama, T. *et al.* Large voltage-induced magnetic anisotropy change in a few atomic layers of iron. *Nat. Nanotechnol.* **4**, 158–161 (2009).
19. D'Souza, N., Salehi Fashami, M., Bandyopadhyay, S., & Atulasimha, J. Experimental clocking of nanomagnets with strain for ultralow power Boolean logic. *Nano Lett.* **16**, 1069–1075 (2016).
20. Ralph, D. C. & Stiles, M. D. Spin transfer torques. *J. Magn. Magn. Mater.* **320**, 1190–1216 (2008).
21. Cui, J. *et al.* A method to control magnetism in individual strain-mediated magnetoelectric islands. *Appl. Phys. Lett.* **103**, 232905 (2013).
22. Biswas, A. K., Ahmad, H., Atulasimha, J. & Bandyopadhyay, S. Experimental demonstration of complete 180 reversal of magnetization in isolated co nanomagnets on a pmn–pt substrate with voltage generated strain. *Nano Lett.* **17**, 3478–3484 (2017).
23. Zhao, Z. *et al.* Giant voltage manipulation of MgO-based magnetic tunnel junctions via localized anisotropic strain: A potential pathway to ultra-energy-efficient memory technology. *Appl. Phys. Lett.* **109**, 092403 (2016).
24. Al-Rashid, M. M., Bandyopadhyay, S. & Atulasimha, J. Dynamic error in strain-induced magnetization reversal of nanomagnets due to incoherent switching and formation of metastable states: A size-dependent study. *IEEE Trans. Electron Dev.* **63**, 3307–3313 (2016).
25. Roy, K., Bandyopadhyay, S. & Atulasimha, J. Hybrid spintronics and straintronics: A magnetic technology for ultra low energy computing and signal processing. *Appl. Phys. Lett.* **99**, 063108 (2011).
26. Ahmad, H., Atulasimha, J. & Bandyopadhyay, S. Reversible strain-induced magnetization switching in FeGa nanomagnets: Pathway to a rewritable, non-volatile, non-toggle, extremely low energy straintronic memory. *Sci. Rep.* **5**, 1–7 (2015).
27. Bandyopadhyay, S., Atulasimha, J. & Barman, A. Magnetic straintronics: Manipulating the magnetization of magnetostrictive nanomagnets with strain for energy-efficient applications. *Appl. Phys. Rev.* **8**, 041323 (2021).
28. Weisheit, M. *et al.* Electric field-induced modification of magnetism in thin-film ferromagnets. *Science*. **315**, 349–351 (2007).
29. Niranjan, M. K., Duan, C. G., Jaswal, S. S. & Tsymbal, E. Y. Electric field effect on magnetization at the Fe/MgO (001) interface. *Appl. Phys. Lett.* **96**, 222504 (2010).
30. Heron, J. T. *et al.* Deterministic switching of ferromagnetism at room temperature using an electric field. *Nature* **516**, 370–373 (2014).
31. Atulasimha, J. & Bandyopadhyay, S. Bennett clocking of nanomagnetic logic using multiferroic single-domain nanomagnets. *Appl. Phys. Lett.* **97**, 173105 (2010).
32. Shiota, Y. *et al.* Evaluation of write error rate for voltage-driven dynamic magnetization switching in magnetic tunnel junctions with perpendicular magnetization. *Appl. Phys. Express.* **9**, 013001 (2015).
33. Grezes, C. *et al.* Ultra-low switching energy and scaling in electric-field-controlled nanoscale magnetic tunnel junctions with high resistance-area product. *Appl. Phys.Lett.* **108**, 012403 (2016).
34. Nowak, J. J. *et al.* Dependence of voltage and size on write error rates in spin-transfer torque magnetic random-access memory. *IEEE Magn. Lett.* **7**, 1–4 (2016).
35. Ishigaki, T. *et al.* A multi-level-cell spin-transfer torque memory with series-stacked magnetotunnel junctions. In *Symposium on VLSI Technology*. 47–48. https://doi.org/10.1109/VLSIT.2010.5556126 (2010).
36. Kim, Y., Fong, X., Kwon, K. W., Chen, M. C. & Roy, K. Multilevel spin-orbit torque MRAMs. *IEEE Trans. Electron Dev.* **62**, 561–568 (2014).
37. Roessler, U. K., Bogdanov, A. N. & Pfleiderer, C. Spontaneous skyrmion ground states in magnetic metals. *Nature.* **442**, 797–801 (2006).
38. Fert, A., Cros, V. & Sampaio, J. Skyrmions on the track. *Nat. Nanotechnol.* **8**, 152–156 (2013).
39. Komineas, S. & Papanicolaou, N. Skyrmion dynamics in chiral ferromagnets. *Phys. Rev. B* **92**, 064412 (2015).
40. Tomasello, R. *et al.* A strategy for the design of skyrmion racetrack memories. *Sci. Rep.* **4**, 1–7 (2014).
41. Iwasaki, J., Mochizuki, M. & Nagaosa, N. Current-induced skyrmion dynamics in constricted geometries. *Nat. Nanotechnol.* **8**, 742–747 (2013).
42. Bhattacharya, D., Al-Rashid, M. M. & Atulasimha, J. Voltage controlled core reversal of fixed magnetic skyrmions without a magnetic field. *Sci. Rep.* **6**, 1–6 (2016).
43. Bhattacharya, D. *et al.* Creation and annihilation of non-volatile fixed magnetic skyrmions using voltage control of magnetic anisotropy. *Nature Electron.* **3**, 539–545 (2020).
44. Rajib, M.M., Al Misba, W., Bhattacharya, D., Garcia-Sanchez, F., & Atulasimha, J. Dynamic skyrmion-mediated switching of perpendicular MTJs: Feasibility analysis of scaling to 20 nm with thermal noise. *IEEE Trans. Electron Dev.* **67**, 3883–3888 (2020).
45. Rajib, M. M., Misba, W. A., Bhattacharya, D. & Atulasimha, J. Robust skyrmion mediated reversal of ferromagnetic nanodots of 20 nm lateral dimension with high Ms and observable DMI. *Sci. Rep.* **11**, 20914 (2021).
46. Schuman, C. D. *et al.* Opportunities for neuromorphic computing algorithms and applications. *Nat. Comput. Sci.* **2**, 10–19 (2022).
47. Rajib, M.M., Al Misba, W., Chowdhury, M.F.F., Alam, M.S., & Atulasimha, J. Skyrmion based energy-efficient straintronic physical reservoir computing. *Neuromorphic Comput. Eng.* **2**, 044011 (2022).
48. Li, C. *et al.* Analogue signal and image processing with large memristor crossbars. *Nat. Electron.* **1**, 52–59 (2018).
49. Hu, M. *et al.* Dot-product engine for neuromorphic computing: Programming 1T1M crossbar to accelerate matrix-vector multiplication. In *Proceedings of the 53rd Annual Design Automation Conference*. 1–6. https://doi.org/10.1145/2897937.2898010 (2016).
50. Bhowmik, D. *et al.* On-chip learning for domain wall synapse based fully connected neural network. *J. Magn. Magn. Mater.* **489**, 165434 (2019).
51. Al Misba, W., Lozano, M., Querlioz, D., & Atulasimha, J. Energy efficient learning with low resolution stochastic domain wall synapse for deep neural networks. *IEEE Access*. **10**, 84946–84959 (2022).
52. Leonard, T. *et al.* Shape-dependent multi-weight magnetic artificial synapses for neuromorphic computing. *Adv. Electron. Mater.* **8**, 2200563 (2022).
53. Wang, P. *et al.* Three-dimensional NAND flash for vector–matrix multiplication. *IEEE Trans. Very Large Scale Integr. Syst.* **27**, 988–991 (2018).
54. Yao, P. *et al.* Fully hardware-implemented memristor convolutional neural network. *Nature.* **577**, 641–646 (2020).
55. Ielmini, D. & Wong, H. S. P. In-memory computing with resistive switching devices. *Nat. Electron.* **1**, 333–343 (2018).
56. Gallo, M. L. *et al.* Mixed-precision in-memory computing. *Nat. Electronics* **1**, 246–253 (2018).
57. Ambrogio, S. *et al.* Equivalent-accuracy accelerated neural-network training using analogue memory. *Nature.* **558**, 60–67 (2018).
58. Jung, S. *et al.* A crossbar array of magnetoresistive memory devices for in-memory computing. *Nature.* **601**, 211–216 (2022).
59. Wong, H. S. P. and S. Salahuddin, S. Memory leads the way to better computing. *Nat. Nanotechnol.* **10**, 191–194 (2015).
60. Chen, S. *et al.* All-electrical skyrmionic magnetic tunnel junction. *Nature* **627**(8004), 522–527 (2024).

61. Urrestarazu Larrañaga, J. *et al.* Electrical detection and nucleation of a magnetic Skyrmion in a magnetic tunnel junction observed via operando magnetic microscopy. *Nano Lett.* **24**(12), 3557–3565 (2024).
62. Zhang, X. *et al.* Skyrmions in magnetic tunnel junctions. *ACS Appl. Mater. Interfaces.* **10**, 16887–16892 (2018).
63. Amiri, P. K. *et al.* Electric-field-controlled magnetoelectric RAM: Progress, challenges, and scaling. *IEEE Trans. Magn.* **51**, 1–7 (2015).
64. Wang, X. S., Yuan, H. Y. & Wang, X. R. A theory on skyrmion size. *Commun. Phys.* **1**, 31 (2018).
65. Bhattacharya, D. & Atulasimha, J. Skyrmion-mediated voltage-controlled switching of ferromagnets for reliable and energy-efficient two-terminal memory. *ACS Appl. Mater. Interfaces.* **10**, 17455–17462 (2018).
66. Zhang, S. L., Van Der Laan, G. & Hesjedal, T. Direct experimental determination of the topological winding number of skyrmions in Cu2OSeO3. *Nat. Commun.* **8**, 14619 (2017).
67. Das, D., Cen, Y., Wang, J. & Fong, X. Bilayer-skyrmion-based design of neuron and synapse for spiking neural network. *Phys. Rev. Appl.* **19**(2), 024063 (2023).
68. Huang, Y., Kang, W., Zhang, X., Zhou, Y. & Zhao, W. Magnetic skyrmion-based synaptic devices. *Nanotechnology* **28**(8), 08LT02 (2017).
69. Wang, M. *et al.* Current-induced magnetization switching in atom-thick tungsten engineered perpendicular magnetic tunnel junctions with large tunnel magnetoresistance. *Nat. Commun.* **9**, 671 (2018).
70. Soni, S., Verma, G. & Kaushik, B. K. Energy efficient ternary computation unit using differential spin Hall effect MRAM. *Semicond. Sci. Technol.* **38**(2), 025005 (2022).
71. Salehi, S., Mashhadi, M. B., Zaeemzadeh, A., Rahnavard, N. & DeMara, R. F. Energy-aware adaptive rate and resolution sampling of spectrally sparse signals leveraging VCMA-MTJ devices. *IEEE J. Emerg. Select. Top. Circ. Syst.* **8**(4), 679–692 (2018).
72. Nehra, V., Prajapati, S., Kumar, T. N. & Kaushik, B. K. High-performance computing-in-memory architecture using STT-/SOT-based series triple-level cell MRAM. *IEEE Trans. Magn.* **57**(8), 1–12 (2021).
73. Cao, Q. *et al.* Nonvolatile multistates memories for high-density data storage. *ACS Appl. Mater. Interfaces.* **12**, 42449–42471 (2020).
74. Sura, A., & Nehra, V. Performance comparison of single level STT and SOT MRAM cells for cache applications. In *25th International Symposium on VLSI Design and Test (VDAT). IEEE.* 1–4; https://doi.org/10.1109/VDAT53777.2021.9601129 (2021).
75. Vansteenkiste, A. *et al.* The design and verification of MuMax3. *AIP Adv.* **4**, 107133 (2014).
76. Alzate Vinasco, J.G. Voltage-controlled magnetic dynamics in nanoscale magnetic tunnel junctions. Doctoral dissertation, UCLA (2014).
77. Shao, Y. *et al.* Sub-volt switching of nanoscale voltage-controlled perpendicular magnetic tunnel junctions. *Commun. Mater.* **3**(1), 87 (2022).
78. Concaa, A. *et al.* Low spin-wave damping in amorphous Co40Fe40B20 thin films. *J. Appl. Phys.* **113**, 213909 (2013).
79. Devolder, T. *et al.* Exchange stiffness in ultrathin perpendicularly magnetized CoFeB layers determined using the spectroscopy of electrically excited spin waves. *J. Appl. Phys.* **120**, 183902 (2016).
80. Cao, A. *et al.* Enhanced interfacial Dzyaloshinskii—Moriya interactions in annealed Pt/Co/MgO structures. *Nanotechnology.* **31**, 155705 (2020).
81. Sajitha, E. P. *et al.* Magnetization dynamics in CoFeB buffered perpendicularly magnetized Co/Pd multilayer. *IEEE Trans. Magn.* **46**, 2056–2059 (2010).
82. Kato, Y. *et al.* Giant voltage-controlled magnetic anisotropy effect in a crystallographically strained CoFe system. *Appl. Phys. Express.* **11**, 053007 (2018).
83. Huang, S. X., Chen, T. Y. & Chien, C. L. Spin polarization of amorphous CoFeB determined by point-contact Andreev reflection. *Appl. Phys. Lett.* **92**, 242509 (2008).
84. Igarashi, J. *et al.* Single-nanometer CoFeB/MgO magnetic tunnel junctions with high-retention and high-speed capabilities. *NPJ Spintronics* **2**(1), 1 (2024).

Acknowledgements

M. M. R. and J. A. would like to acknowledge US National Science Foundation CISE SHF Small grant # 1909030 and VCU Breakthroughs Fund: Energy Efficient Neurocomputer. N.B., R. K. R. and B. K. K would like to acknowledge Science and Engineering Research Board (SERB), Department of Science and Technology, Government of India under Grant CRG/2019/004551 for providing the funding to carry out the research work.

Author contributions

The study was conceived and designed by Author M.M.R. and J.A. Author M.M.R. performed the simulation. Author N.B, R.K.K. performed the energy calculation. Author M.M.R. drafted the manuscript to which all co-authors contributed.

Competing interests

The authors declare no competing interests.

Additional information

Supplementary Information The online version contains supplementary material available at https://doi.org/10.1038/s41598-024-66853-w.

Correspondence and requests for materials should be addressed to J.A.

Reprints and permissions information is available at www.nature.com/reprints.

Publisher's note Springer Nature remains neutral with regard to jurisdictional claims in published maps and institutional affiliations.